CO$_2$ Adsorption Capacities in Zeolites and Layered Double Hydroxide Materials

Cristina Megías-Sayago[1]*, Rogéria Bingre[1], Liang Huang[1,2], Gaëtan Lutzweiler[3], Qiang Wang[2] and Benoît Louis[1]

[1] ICPEES – Institut de Chimie et Procédés pour l'Energie, l'Environnement et la Santé, Energy and Fuels for a Sustainable Environment Team, UMR 7515 CNRS – Université de Strasbourg – ECPM, Strasbourg, France, [2] Environmental Functional Nanomaterials (EFN) Laboratory, College of Environmental Science and Engineering, Beijing Forestry University, Beijing, China, [3] INSERM, UMR 1121, Strasbourg, France

The development of technologies that allow us to reduce CO$_2$ emissions is mandatory in today's society. In this regard, we present herein a comparative study of CO$_2$ adsorption over three types of materials: zeolites, layered double hydroxides (LDH), and zeolites coated LDH composites. The influence of the zeolite Si/Al ratio on zeolites sorption capacity along with the presence of mesopores was investigated. By comparing these results with the well-known performance of LDHs, we aim to provide insights on the factors that may influence the CO$_2$ capture capacity over zeolites, thus providing useful tools for tuning their properties upon post-treatments.

Keywords: CO$_2$ adsorption, zeolite, LDH, zeolite@ LDH, Si/Al, hierarchical porosity

INTRODUCTION

The tremendous increase in the use of fossil fuels in the past 200 years has contributed to a steady rise of CO$_2$ level in the atmosphere (Smil, 2017). Being the main actor responsible for the greenhouse effect, it led to reach a global warming never seen before, coming close to the pessimistic scenario (Stanley, 2003). Several efforts have been made to reduce those emissions, either by optimization of the current industrial processes, or by implementation of renewable energies where no CO$_2$ is produced (Princiotta, 2011; Álvarez et al., 2017). However, the latter remain at a non-sufficiently mature state, hampered by high costs for their implementation and maintenance, mainly in developing countries (Mustapa et al., 2010; Horbach et al., 2014). Hence, this leads to the need to continue depleting fossil fuels to generate energy, and consequently, allow further release of CO$_2$ in the atmosphere. Unfortunately, fossil fuels are not the unique factor increasing carbon footprint nowadays. A significant contribution comes from several industrial activities such as cement or steel production, whose CO$_2$ emissions dramatically contribute to accelerate climate change.

CO$_2$ capture technologies have been recently implemented in industries. However, the sole commercially mature technology to capture CO$_2$ remains an amine-based scrubbing, but its high cost and hazardous by-products forces mankind to find out alternative technologies (Veltman et al., 2010; Vericella et al., 2015; Chen C. et al., 2017).

The development of new solid adsorbents / sorbents has flourished in the last decade, being preceded by Sircar's group work (Sircar et al., 1996). The latter sorbents can be classified into low-temperature (< 200°C), intermediate-temperature (200–400°C), and high-temperature (> 400°C) CO$_2$ adsorbents/sorbents depending on their working temperature range (Wang et al., 2012, 2015; Cao et al., 2014). LDH, known as hydrotalcite-like compounds, are a class of layered

materials which comprise mono- or di- and trivalent cations. To date, several studies have been dealing with the high potential of LDHs-derived CO_2 adsorbents, especially conventional Mg-Al LDHs, which demonstrated a great performance at high temperatures (Alpay and Ding, 2000; Hutson and Attwood, 2008; Sharma et al., 2008; Lwin and Abdullah, 2009; Chang et al., 2013). Likewise, zeolites have also been subjected to extensive research for the adsorption of CO_2 due to their high capture capacity, low regeneration temperatures and high stability over several adsorption-desorption cycles (Siriwardane et al., 2005; Pham et al., 2014; Bande et al., 2015; Chen C. et al., 2017; Hasegawa and Matsumoto, 2017). Regarding sorbents working at intermediate temperature range, recent studies have shown a great potential from LDH coated zeolites (Li et al., 2018). A considerable increase in the adsorption of CO_2 was observed after the coating of LDH over a zeolite core at temperatures ranging from 30 to 300°C (Othman et al., 2006).

Herein, we present a CO_2 adsorption study comprising the three types of aforementioned materials. The impact of the zeolite Si/Al ratio on its capture capacity, as well as the presence of mesopores has been highlighted. By comparing these results with the well-known performance of LDHs and LDH@zeolite composites, we aim to give insights on the factors that may influence the CO_2 capture in zeolites, thus providing useful tools to tune their features upon different post-treatments (LDH coating, introduction of mesoporosity).

EXPERIMENTAL

Synthesis

Large Crystal Zeolites

NH_4-ZSM-5 zeolites were directly synthesized via fluoride-mediated route adapted from our former studies. In a typical synthesis, the Al-source (different amounts to reach the following Si/Al molar ratios: 200, 100, 50, and 25) was first weighted in a 150 mL-Erlenmeyer flask where 50 mL of distilled water was added under vigorous stirring (700 rpm, r.t.). After complete dissolution, TPABr (0.498 g) and NH_4F (1.103 g) were consecutively added. Finally, 1.607 g of solid silica (Aeroperl 300/30, Evonik) was slowly added during 5 min. The gel was aged 2 h under vigorous stirring and finally autoclaved at 443 K for 144 h. H-zeolite form was easily obtained after a single calcination at 823 K during 15 h in static air, needed to completely remove the template. The samples were named as H-ZSM-5-A, H-ZSM-5-B, H-ZSM-5-C and H-ZSM-5-D, respectively, following the order related with the Si/Al molar ratio (usually denoted as SAR) decrease.

Zeolite Derived Materials

Commercial ZSM-5 zeolite (CBV3020E) having Si/Al molar ratio of 15 was purchased from Zeolyst in its ammonium form. The zeolite was either calcined at 600°C for 4 h to produce its proton form, named R0-H, or subjected to a cationic exchange to produce its sodium form R0-Na. The latter was performed by exchanging three times the zeolite with NaCl 1 M at 80°C for 1h, followed by filtration and drying. To prepare the mesoporous zeolite, 200 mg of the commercial powder in its proton form was

subjected to an alkaline treatment with 0.15 mL of 0.2 M of NaOH at 65°C for 30 min. The solution was filtered, dried and added to a 30 mL solution of tetraethylammonium hydroxide (TEAOH, 0.1 M) and 100 mg of alkali lignin (Aldrich). After stirring, the solution was transferred to an autoclave and placed in an oven at 150°C for 10 h, followed by filtration, drying and calcination at 550°C for 15 h (1 h ramp to burn off the templates). The sample was treated three times with 1 M of NH_4Cl at 80°C, followed by filtration, drying and calcination at 550°C to release NH_3 to ensure the proton form of the zeolite. The sample was named R0-meso-H. Following the same procedure as for R0-H, the mesoporous sample was subjected to another cationic exchange to leave its sodium form R0-meso-Na.

R0-H material was also coated with Mg-Al LDH using a co-precipitation method. It should be noted that based on the obtained results (H-ZSM-5-D vs. R0-H), only the commercial sample was chosen for the coating procedure. Firstly, 200 mg of zeolite was dispersed in 40 mL of distilled water for 30 min, followed by the addition of 0.212 g of sodium carbonate and dispersion for additional 20 min. Then, a 40 mL aqueous solution containing 1.918 mmol of magnesium nitrate hexahydrate ($Mg(NO_3)_2.6H_2O$) and 0.955 mmol of aluminium nitrate nonahydrate ($Al(NO_3)_3.9H_2O$) was added drop-wise to the previous solution for around 1 h under vigorous stirring. The pH of the solution was kept constant at 10 by adding 1 M of sodium hydroxide. After stirring for 4 h, the solid was filtered and washed. The sample was stirred for another 4 h in 40 mL of ethanol, and then filtered and dried. The composite was calcined at 400°C for 5 h to obtain the LDO (layered double oxide) and named finally R0@LDH.

LDHs

MgAl and CaAl LDHs were prepared using the co-precipitation method. All chemicals were purchased from Acros Organics, VWR and Sigma-Aldrich. In brief, a salt solution containing a mixture of M^{2+} precursor and $Al(NO_3)_3$ $9H_2O$ was added dropwise to an alkaline solution (100 mL) containing Na_2CO_3 ($NaNO_3$ for CaAl LDHs) and additives. The pH of the precipitation solution was kept constant at 10 (or 11 for CaAl LDHs) by addition of NaOH (4M) solution. The resulting mixture was aged at room temperature for 12 h under continuous stirring. The aged mixture was then filtered and washed with deionized water followed by drying at 100°C in an oven. In order to study the impact of structural degradation (LDO formation), MgAl LDH sample was finally calcined at 400°C during 5 h in static air. Meanwhile, CaAl LDH was treated at 750°C during 5 h in the same atmosphere. Samples were named as LDH fresh or LDH calcined.

Characterization

Powder X-ray diffraction (XRD) patterns of zeolites were acquired using a Bruker D8 (Cu Kα) diffractometer operated at 40 kV and 40 mA. XRD patterns were recorded in the 2θ = 5–60° range with a step size of 0.05°. XRD patterns of LDH materials were acquired over a Rigaku Ultima IV apparatus using CuKα radiation (λ = 0.15418 nm), operated at 40 kV and 20 mA. Scans were performed at 2° min^{-1} in the 3–70° range.

SEM images were acquired in a JEOL FEG-6700F microscope working at a 9 kV accelerating voltage. Bulk elemental analyses were determined by X-ray fluorescence (XRF) using a XEPOS (AMETEK) device equipped with a Rh radiation tube.

The textural properties were analyzed by means of nitrogen physisorption using Micromeritics ASAP 2420 equipment. Samples were pre-treated *in-situ* at 200°C under vacuum prior to the analyses. Surface areas were determined using the BET method and pore size distributions were obtained using the adsorption branch of the isotherms (BJH method).

Zeolite acid site density was evaluated by temperature programmed ammonia desorption (NH_3-TPD) by using a Micromeritics AutoChem II chemisorption analyzer equipped with TCD detector. Samples were pre-treated *in-situ* at 550°C during 1 h under helium atmosphere. After that, samples were cooled down to room temperature and a 5% NH_3/He flow was passed through the reactor. Once physisorbed ammonia was removed, the temperature gradually increased to 550°C.

The hydrophilicity of the zeolites has been determined by contact angle measurements as follows: 20 mg of powder was placed under an hydraulic press, and let under 12 bar for 30 s to obtain a compact pellet. Wetting properties of the samples were determined by static contact angle using an optical tensiometer (Attension theta, Biolin Scientific). A 2 μl drop of purified water (milli Q) was deposited on the pellet surface and the angle was recorded by the camera mounted on the device.

Evaluation of CO_2 Adsorption Capacity

Thermogravimetric sorption of CO_2 on zeolites, LDHs and composites was measured using a TGA analyzer (Q500 TA Instrument). All solids were first calcined in a muffle furnace at a temperature comprised between 400 and 600°C for 5 h, before transferring the samples to the TGA analyzer. To avoid any error, the test was done immediately after the first calcination. Finally, the samples were further calcined *in situ* for 1 h in N_2 prior to the measurement. CO_2 adsorption experiments were carried out at 1 atm with a constant flow of CO_2 (40 mL min^{-1}).

RESULTS AND DISCUSSION

Large Zeolite Crystals

Fluoride-mediated synthesis of ZSM-5 zeolite crystals provides mild conditions, thus facilitating the formation of few nuclei under diluted conditions as consequence of a slow release of $SiO_xF_y^-$ species (Flanigen et al., 1986; Losch et al., 2017). The latter renders possible the formation of highly crystalline zeolites characterized by larger crystals (usually tenths of microns) with less defects and more open structures than in alkaline medium (Xu et al., 1990). This, together with the high Si/Al ratio that can be obtained, entails the formation of more

TABLE 1 | Chemical composition, acid site density and textural properties of as-synthetized H-ZSM-5 zeolites.

Sample	SAR (XRF)	Acid site density (mmol(H$^+$)/g zeolite)[a]	S$_{BET}$ [m^2/g]	V$_{pore}$ (cm^3/g)
H-ZSM-5-A	226	0.110	355	0.178
H-ZSM-5-B	115	0.168	296	0.184
H-ZSM-5-C	55	0.297	348	0.178
H-ZSM-5-D	43	0.309	347	0.181

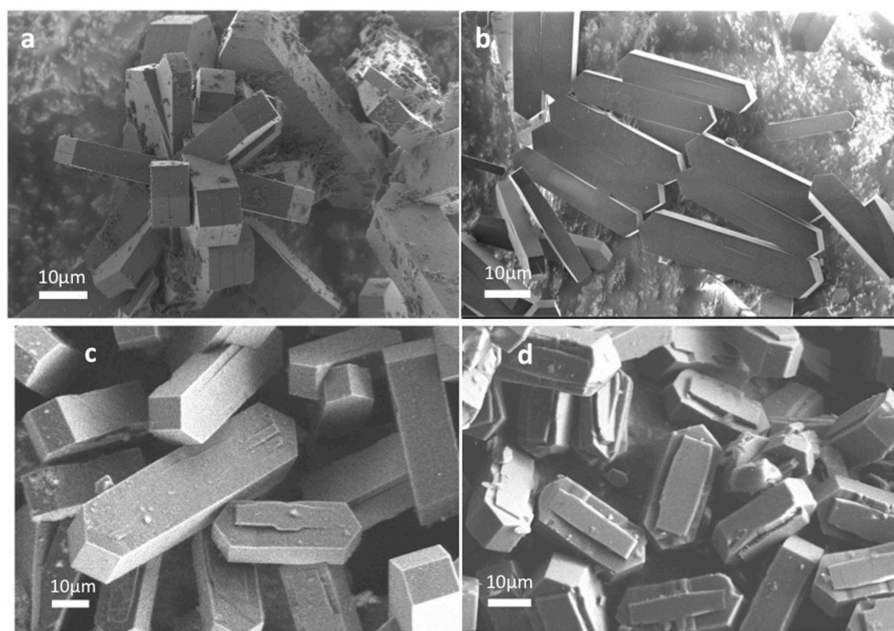[a] Determined by NH_3-TPD.

FIGURE 1 | SEM images of as-synthetized H-ZSM-5 zeolites. **(a)** H-ZSM-5-A, **(b)** H-ZSM-5-B, **(c)** H-ZSM-5-C, and **(d)** H-ZSM-5-D.

hydrophobic materials. Therefore, the possible effect of both the hydrophobicity and crystal size can be evaluated in terms of CO_2 capture capacity.

The XRD patterns of each zeolite (**Figure S1**) confirmed the presence of the sole MFI structure (Ocampo et al., 2009, 2010). Whatever the aluminum content in the framework, all syntheses led to the formation of large prismatic crystals (**Figure 1**) having between 30 and 60 μm in size. Lower Al containing zeolites have, in general, narrow crystal size distributions (**Figures 1a,b**) differing from zeolites with higher Al content (**Figure 1c**). A difference in the crystal morphology can be observed for H-ZSM-5-D (possessing the lowest SAR, **Table 1**).

Table 1 summarizes the Si/Al ratios, the total number of Brønsted acid sites and the textural properties of as-prepared zeolites. XRF values together with NH_3-TPD experiments confirm a successful variation of acidic properties, i.e., aluminum content, within the series while neither influencing the specific surface areas, nor the pore volumes.

CO_2 capture capacities of large crystals H-ZSM-5 zeolites were evaluated using a TGA analyzer in order to monitor the weight changes of each sample under a constant CO_2 flow. Prior to analysis, the sample surface was cleaned by means of two calcination steps *in situ* under inert flow. Afterwards, CO_2 capture abilities were evaluated at low temperature (40°C) and intermediate-temperature (200°C) and presented in **Figure 2**. The data acquired at low temperature strongly depend on the Si/Al content in zeolites (**Figure 2A**) which is in agreement with former literature reports (Chen H. et al., 2017). CO_2 adsorption capacity was enhanced while diminishing the Si/Al ratio. This can be attributed to the presence of more Al-atoms in the framework. CO_2 interaction with zeolites is governed by the hard Lewis base character of oxygen atoms (Pham et al., 2014) that strongly interact with hard Lewis acid sites as Al^{3+}. One may therefore *a priori* expect that lower Si/Al ratio may induce a higher quantity of CO_2 adsorbed. Indeed this trend could be verified over large MFI zeolite crystals. In addition, lower Si/Al implies superior ion exchange ability due to the presence of more charge compensation cations. Finally, zeolites with lower Si/Al ratio are expected to be more hydrophilic. Indeed, contact angle measurements have been performed and hopefully confirmed this statement. H-ZSM-5-D, having the lowest SAR (43), exhibited the smaller contact angle with the water drop, 22.6° in comparison with 28.5° for H-ZSM-5-C (SAR 55), 55.0° for H-ZSM-5-B (SAR 115) and 67.0° for H-ZSM-5-A (SAR 226), respectively.

To summarize, the higher CO_2 sorption capacity has been obtained over zeolites which are more hydrophilic, thus possessing more Al-atoms in the frame.

The adsorption capacity at intermediate-temperature (200°C) was also evaluated over H-ZSM-5-D (lowest SAR zeolite) and presented in **Figure 2A**. The adsorption capacity diminished from 1.033 to 0.056 $mmol_{CO2}$/g, limiting the application of large ZSM-5 crystals at higher temperatures. The latter result points out the importance of physisorption phenomena in zeolites at low temperatures. In contrast at higher temperatures, CO_2 sorption should be only ruled by
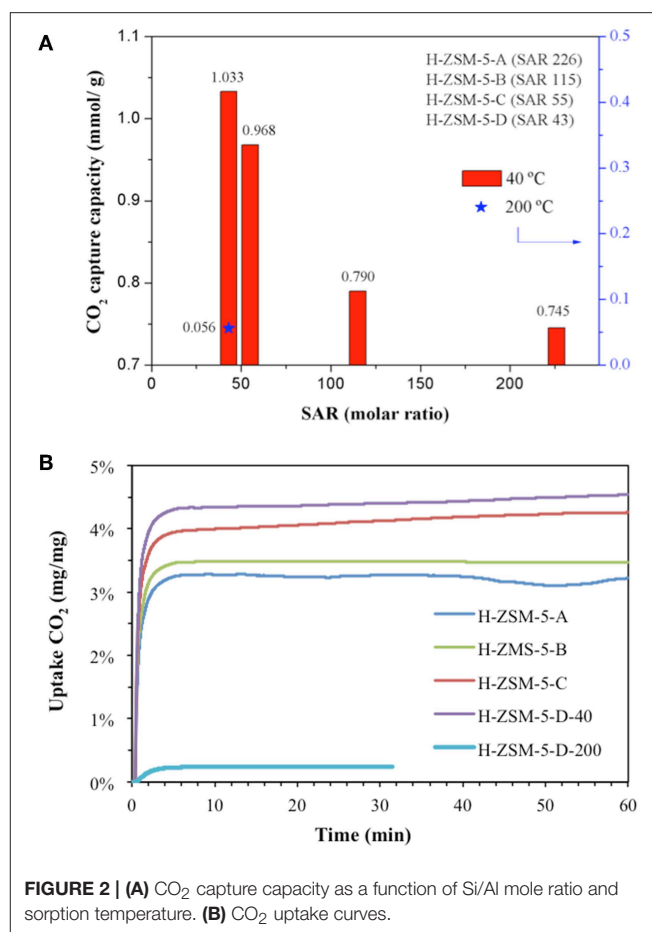

FIGURE 2 | (A) CO_2 capture capacity as a function of Si/Al mole ratio and sorption temperature. **(B)** CO_2 uptake curves.

chemical interactions, which unfortunately diminishes the sorption capacity.

CO_2 uptake curves as function of time are shown in **Figure 2B**. The sorbents displayed fast CO_2 sorption kinetics for a very short absorption time period (less than 3 min). The latter could be attributed to the high specific surface area and the microporous network which provide a higher availability of active sites. In general, two stages concerning the sorption process can be differentiated in the solids. Firstly, a fast uptake reaction occurs at the initial stage of CO_2 absorption (less than 3 min). Secondly, a later long-period stage usually appears where it is possible to distinguish a continuous (but considerably slower) increase in the sample weight. The first stage is directly related to the chemical reaction control whilst the second one is more likely attributed to a diffusional control (Chang et al., 2013). By careful comparing these uptake curves obtained at 40°C (**Figure 2B**), it is noteworthy that the sorption process is controlled by the chemical reaction for low Al content H-ZSM-5-A (SAR 226) and H-ZSM-5-B (SAR 115) zeolites. In contrast, H-ZSM-5-C (SAR 55) and H-ZSM-5-D (SAR 43) seem to suffer from diffusional limitations. These results are in line with the adsorption capacity values presented in **Figure 2A**. As aluminum content increases in the materials, a larger amount of CO_2 molecules diffuse and absorb within the pores, thus hindering the
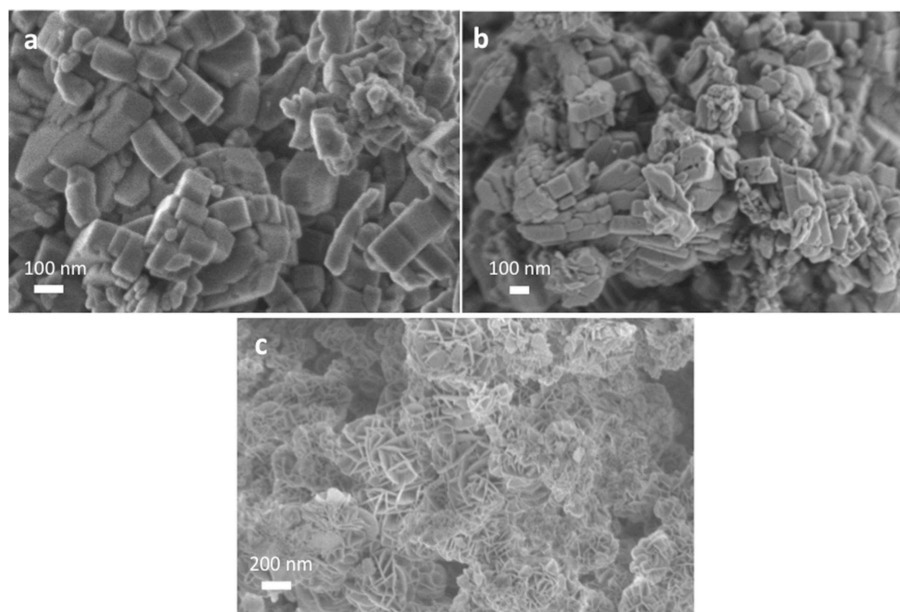
FIGURE 3 | SEM pictures of **(a)** R0-H, **(b)** R0-meso H, and **(c)** R0@LDH composite.

CO_2 diffusion along the cavities. This phenomenon is discarded at 200°C due to the lower uptake capacity at higher temperatures.

Core-Shell LDH@zeolite Composites

The diffraction patterns of commercial R0-H zeolite and core-shell LDH@zeolite material confirm the sole presence of MFI structure (**Figure S2**). Neither the presence of mesopores nor the coating of LDH led to different diffraction peaks. The LDH presence is evidenced by SEM analysis as shown in **Figure 3**. R0-H sample possess regular nanosized morphology (**Figure 3a**) with smooth surface which became rough when the mesopores were created (**Figure 3b**). After coating with LDH, the composite retains the original shape of pristine zeolite together with uniform flower-like shaped edges (**Figure 3c**). A core-shell LDH@ZSM-5 zeolite composite has therefore been successfully obtained, as already reported by Wang et al. (Li et al., 2018).

The textural properties of commercial R0-H and post-modified materials are summarized in **Table 2**. The specific surface area of both zeolites (commercial and meso) is close to 360–370 m^2/g, not being affected by the presence of mesopores. A slight decrease of about 20% in BET surface could be observed after the coating with LDH, R0@LDH sample, whilst the total pore volume almost doubled.
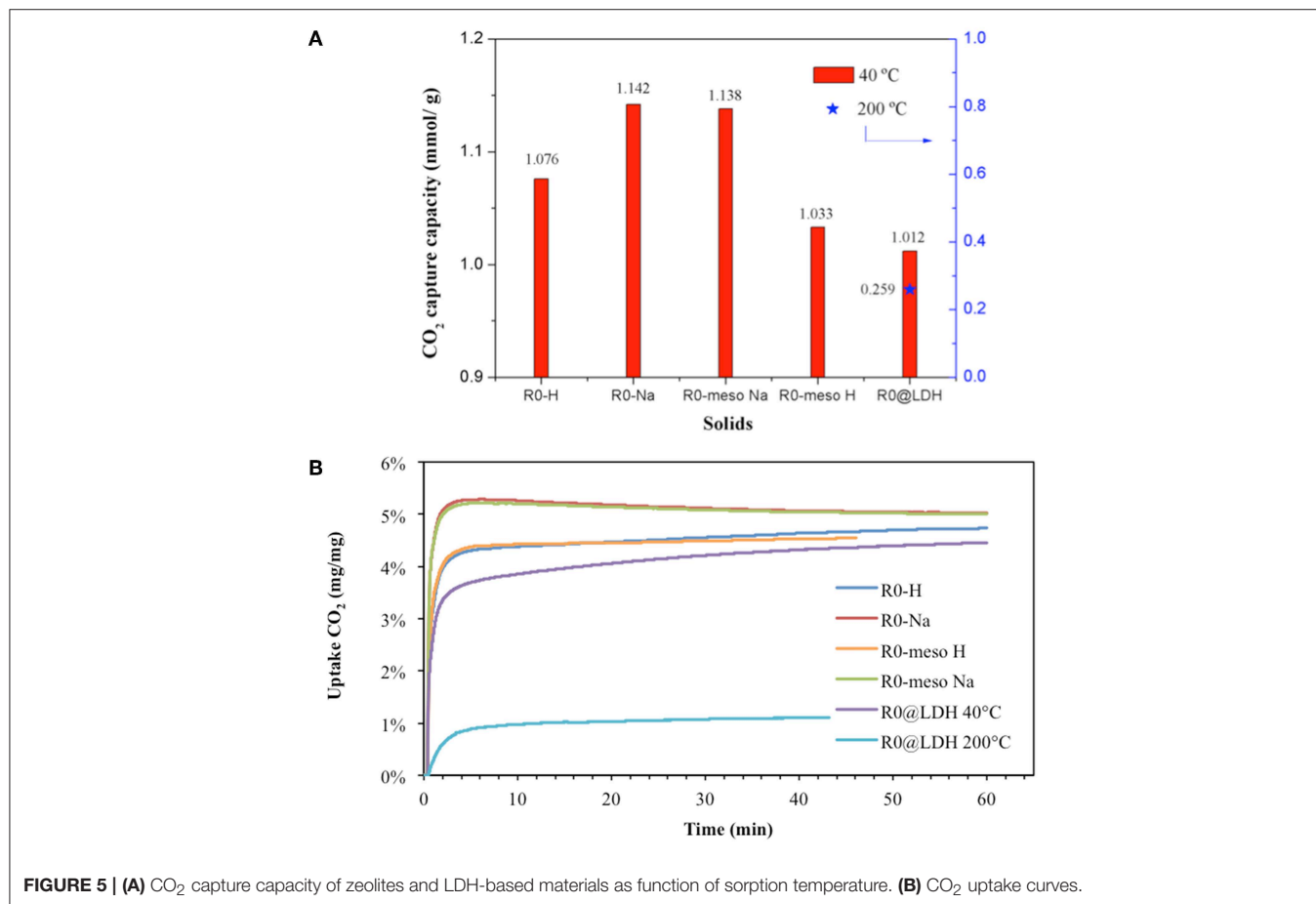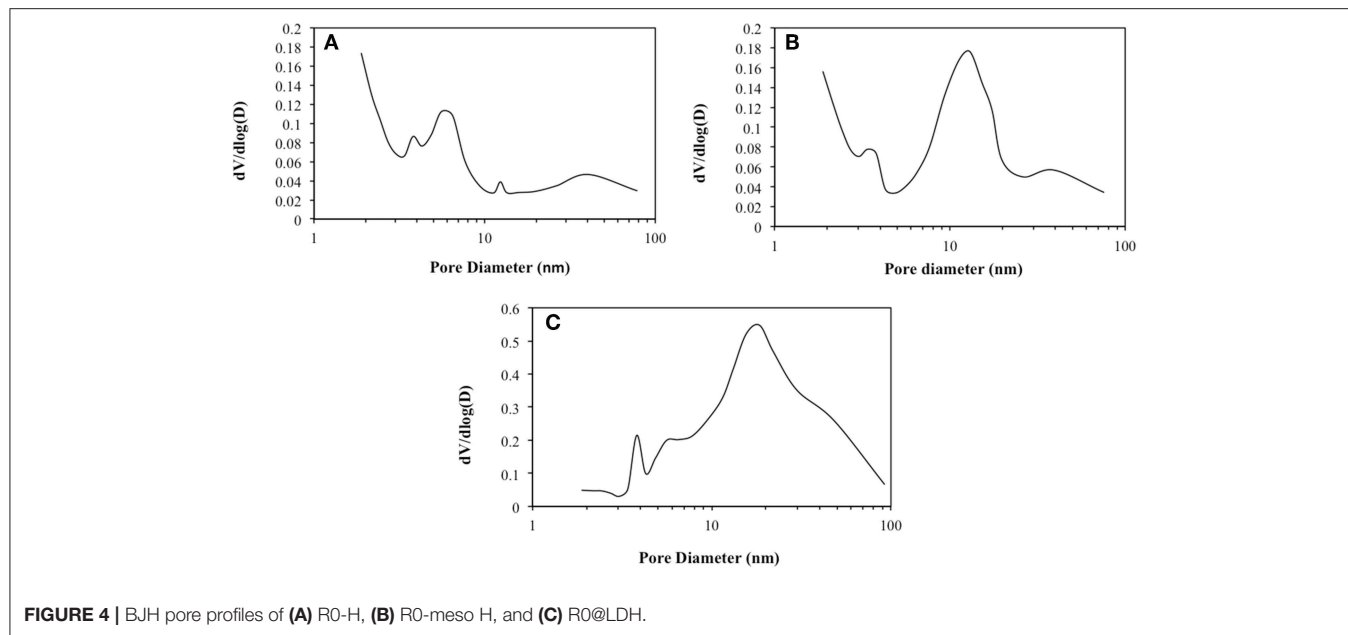
In order to gain more insights on those samples porosity, BJH pore profiles are shown in **Figure 4**. The pore size variation toward the mesoporous range among the samples is verified while ranging from R0-H to R0-meso H and R0@LDH. Pristine zeolite is characterized by the sole presence of micropores (**Figure 4A**) together with mesopores having 4–6 nm being assigned to intercrystalline porosity. The pore diameter profile changes for R0-meso H (**Figure 4B**)

TABLE 2 | Textural properties of commercial R0-H and zeolite derived materials.

Sample	S_{BET} [m^2/g]	S_{meso} [m^2/g]	V_{total} (cm^3/g)	V_{micro} (cm^3/g)
R0-H	369	147	0.23	0.109
R0-meso H	362	144	0.26	0.107
R0@LDH	298	142	0.43	0.076

highlighting the presence of mesopores of about 12 nm, demonstrating the mesoporous character of this sample. Regarding the zeolite coated with LDH (**Figure 4C**), the pore sizes further increased in the mesoporous range. The presence of macropores could also be evidenced, being probably due to the presence of LDHs at the zeolite crystals surface (Li et al., 2018). Zeolite micropores might be still accessible during nitrogen adsorption after the LDH coating procedure but the diffusion might be partially hindered. In any case, the use of zeolite for the synthesis of the LDH@ZSM-5 nanocomposite allows enhancing the specific surface area in comparison to pristine LDH.

CO_2 capture capacities of as-prepared samples are presented in **Figure 5A**. In order to evaluate the cation nature influence along with the mesopore presence, R0-H and R0 meso-H samples were subjected to cationic exchange to get their sodium form. In principle, the CO_2 sorption capacity raises when the protons are exchanged with sodium cations (R0-H vs. R0-Na and R0 meso-H vs. R0 meso-Na, respectively). Although some differences could be observed due to mesopores presence, a higher capacity could be achieved over Na-zeolite forms. Previous studies have underlined that the main interaction between the zeolite surface and CO_2 is the field gradient—quadrupole interaction

FIGURE 4 | BJH pore profiles of **(A)** R0-H, **(B)** R0-meso H, and **(C)** R0@LDH.

FIGURE 5 | **(A)** CO_2 capture capacity of zeolites and LDH-based materials as function of sorption temperature. **(B)** CO_2 uptake curves.

(Hasegawa and Matsumoto, 2017) which is proportional to r^{-3} and the valence of the cation, z. Since the ionic radius of H^+ is the smallest, the ion-CO_2 distance is the shortest and therefore the interaction would be the strongest. Carbon dioxide molecules in small and medium-pore zeolites are strongly adsorbed, possibly hindering the diffusion of other molecules inside the pores, resulting in smaller CO_2 uptake capacities. The latter explains the lower observed uptakes for

acidic R0 and R0-meso samples in comparison to their Na-exchanged counterparts.

The presence of mesopores (R0-H vs. R0-meso H) led to lower sorption capacities, in contrast to what could be expected taking into account mass transfer limitations. A possible explanation could be based on the removal of Al-atoms during the creation of the mesopores, diminishing therefore the number of potential adsorption sites for carbon dioxide molecules. Indeed, the sorption capacity achieved over R0-meso H sample is 1.033 $mmol_{CO_2}$/g, being exactly the same value reached over H-ZSM-5-D. The later zeolite has a Si/Al = 43, which is almost the triple than for R0-H (Si/Al = 15). This effect is partially suppressed after exchanging the zeolite with Na$^+$, probably due to a better diffusion of carbon dioxide molecules through the narrow zig-zag channels, hence enabling an easier access to the active sites.

When the acidic R0 zeolite is coated with LDH, a lower sorption capacity is obtained. As observed in the BJH profiles, zeolite micropores seem to be blocked (at least partially) after LDH coating, suggesting that only the LDH part could interact with CO_2. Although LDHs have demonstrated to be efficient CO_2 adsorbents (Chang et al., 2013), the quantity used in this composite is smaller when compared to bare LDH material. At higher temperature (200°C), the capacity value diminishes from 1.012 to 0.259 $mmol_{CO_2}$/g (which supposes 76% capacity loss), as expected by the exclusion of physisorption phenomenon at higher temperatures. However, this decrement is low in comparison with the 95% registered for H-ZSM-5-D zeolite (previous section) which points out the beneficial effect of LDH coating.

Figure 5B shows the CO_2 uptake curves as a function of time for each sample. It is worthy to mention that Na-exchanged samples and acidic zeolites follow the similar trend, being different from LDH coated sample. All samples are characterized by a fast adsorption process (less than 3 min) followed by a diffusional control effect depending on the material. Slight differences can be observed over micro- and mesoporous H-zeolites (R0-H vs. R0-meso H) regarding the second adsorption stage, i.e., the later long-period stage. For R0-H, it is possible to distinguish a continuous but considerably slower weight increase contrarily to R0-meso H sample. This effect suggests that the mesopores presence may avoid diffusional problems during the adsorption process. Likewise for Na-exchanged samples, a continuous decrease in the sample weight is observed, thus indicating that a small fraction of CO_2 molecules are fastly and weakly adsorbed on the zeolite surface. The impact of diffusion is more pronounced over R0@LDH at 40°C, being limited at 200°C.

LDHs

The diffraction patterns of MgAl and CaAl based samples are presented in **Figure S3**. Highly crystalline Mg-Al-NO$_3$ and Ca-Al-NO$_3$ were successfully prepared using co-precipitation method leading to pure LDHs phases (Wang et al., 2015) with characteristic peaks at 11.7°, 23.7°, 34.7°, and 39.3°, corresponding to the basal planes of (003), (006), (009) and (015) reflections (Climent et al., 2004). Since LDH derived materials will be activated by thermal treatment before CO_2 sorption, XRD patterns were also recorded after calcination. LDHs usually lose their layered structure, turning into layered double oxides (LDOs) which possess three kinds of active sites. The structure and composition changes are probably the most important parameters to take into account for an application as sorbent. It can be deduced from TGA curves (**Figure S4**), that structural changes occur at different temperatures for MgAl and CaAl LDHs. MgAl LDH first loses its interlayer water until 200°C. From this temperature, the dehydroxylation of the octahedral layers takes place as well as the interlayer charge compensation nitrate anions removal, which last up to 400°C. The same two weight loss steps can be differentiated for CaAl LDH, being in this case 550°C the final temperature. Based on that and in order to ensure LDOs formation, MgAl and CaAl LDHs were calcined at 400°C and 750°C during 5 h, respectively, and XRD diffraction patterns presented in **Figure S3**. As expected, after calcination,

TABLE 3 | Textural properties of fresh and calcined LDHs.

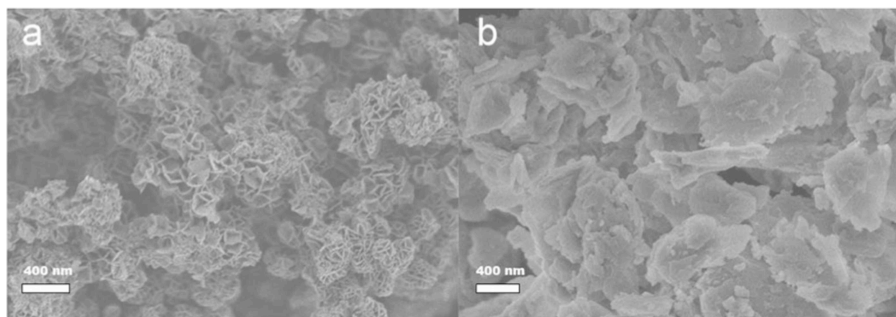| Sample	S_{BET} [m²/g] fresh	S_{BET} [m²/g] calcined	Pore size (nm) fresh	Pore size (nm) calcined	V_{pore} (cm³/g) Fresh	V_{pore} (cm³/g) calcined
MgAl LDH	50	224	9.0	13.3	0.19	0.63
CaAl LDH	21	26	10.4	10.0	0.04	0.06

FIGURE 6 | SEM images of **(a)** MgAl LDH and **(b)** CaAl LDH.

the samples lost their original structure and changed to pure mixed-metal oxide phases, $MgAl_2O_4$ and $CaAl_2O_4$, respectively.

SEM images of LDH samples are presented in **Figure 6**. MgAl LDH exhibits a typical spheroidal rose-like morphology different from CaAl LDH where only regular aggregates could be observed.

The textural properties of fresh (LDH) and calcined (LDOs) solids are presented in **Table 3**. MgAl LDH specific surface area is more than twice higher than CaAl one. In both cases, the S_{BET} increased after calcination, although the increment is much higher for MgAl, reaching 224 m^2/g. The pore sizes are similar for both samples, increasing for MgAl after calcination. Likewise to the pore volume, important differences between the samples could be detected, MgAl exhibiting a much higher pore volume. In both cases, the values increased after calcination, becoming more important for MgAl sample.

Carbon dioxide capacity values are presented for both samples in **Figure 7A**. The superiority of MgAl sample is evidenced at both temperatures, which seems logical taking into account the higher specific surface area and pore volume. Likewise for the uptake curves (**Figure 7B**), both samples are characterized by a fast adsorption (superior to the zeolites) and diffusional impediment in a second stage,

being evidenced by a continuous weight increase as a function of time.

Comparison of the Sorbents

In general, CO_2 sorption capacity depends on different factors as discussed throughout this contribution. A careful control of these
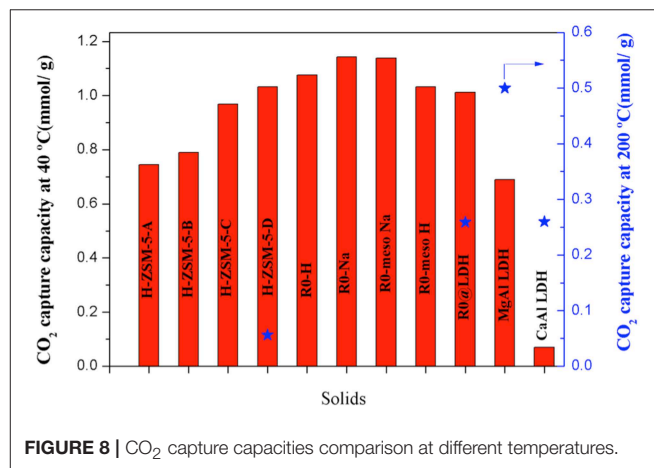

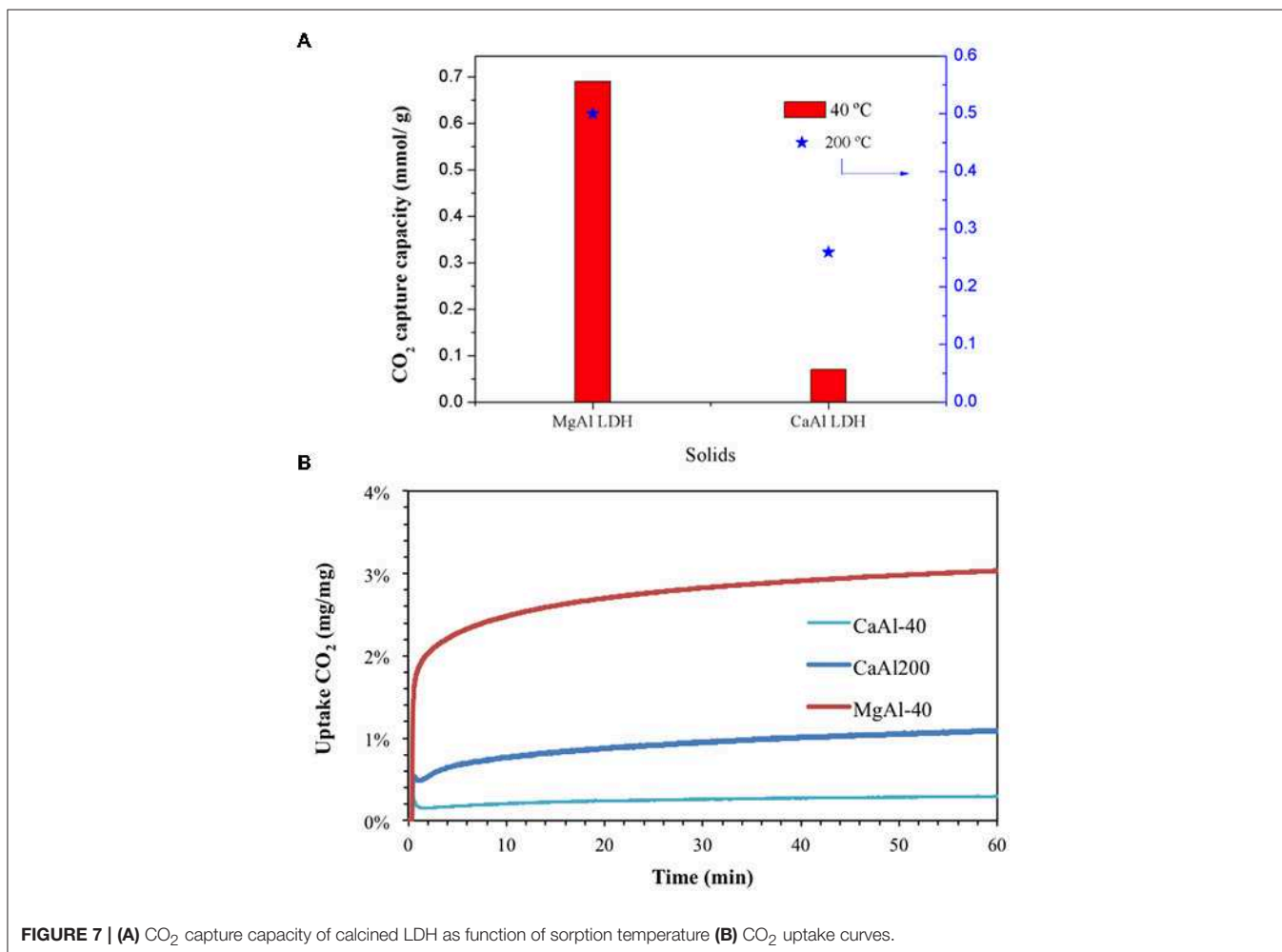**FIGURE 8 |** CO_2 capture capacities comparison at different temperatures.

FIGURE 7 | (A) CO_2 capture capacity of calcined LDH as function of sorption temperature **(B)** CO_2 uptake curves.

parameters for different materials is an effective tool to select the suitable application for the right material.

In order to summarize and properly compare, CO$_2$ capture capacities of all materials are presented in **Figure 8**. At low temperature, the highest sorption values are registered for Na-exchanged zeolites. As aforementioned, the presence of mesopores did not have an important impact, contrarily to the Si/Al ratio and the cation nature. The impact of Si/Al ratio has been demonstrated for the large zeolite crystals (H-ZSM-5-A to H-ZSM-5-D samples). Likewise, the cation nature effect has been evidenced whatever the crystal size. While raising the temperature, the superior performance of LDHs is clear. Although at 40°C, R0@LDH's capacity remained lower than pristine zeolite (R0-H and R0-Na), at higher temperature the LDH coating led to a more efficient sorbent material, comparable to CaAl LDH. Nevertheless, the best potential sorbent at intermediate temperature remains MgAl LDH.

CONCLUSION

The synthesis and characterization of large ZSM-5 zeolite crystals and LDH derived materials have been successfully performed. Those materials demonstrated efficient CO$_2$ sorption capacity. It has been clearly shown that CO$_2$ capture strongly depends on the concentration of Al-atoms in the zeolite framework as well as its cation nature. In contrast, the mesoporous character did not seem to induce an important effect.

For LDHs, high specific surface area combined with high pore volume appear as a determining factor for achieving high adsorption. When comparing different materials, the highest sorption values at low temperature were registered for sodium-exchanged zeolites. When enhancing the temperature up to 200°C, the superiority of LDHs has been clearly evidenced.

DATA AVAILABILITY

All datasets generated for this study are included in the manuscript and/or the **Supplementary Files**.

AUTHOR CONTRIBUTIONS

All authors listed have made a substantial, direct and intellectual contribution to the work, and approved it for publication.

SUPPLEMENTARY MATERIAL

The Supplementary Material for this article can be found online at: https://www.frontiersin.org/articles/10.3389/fchem.2019.00551/full#supplementary-material

REFERENCES

Alpay, E., and Ding, Y. (2000). Equilibria and kinetics of CO$_2$ adsorption on hydrotalcite adsorbent. *Chem. Eng. Sci.* 55, 3461–3474. doi: 10.1016/S0009-2509(99)00596-5

Álvarez, A., Bansode, A., Urakawa, A., Bavykina, A. V., Wezendonk, T. A., Makkee, M., et al. (2017). Challenges in the greener production of formates/formic acid, methanol, and DME by heterogeneously catalyzed CO$_2$ hydrogenation processes. *Chem. Rev.* 117, 9804–9838. doi: 10.1021/acs.chemrev.6b00816

Bande, R. I., Sadhana, R., and Rashami, S. D. (2015). CO$_2$ adsorption and desorption studies for zeolite 4A. *Res. J. Mater. Sci.* 3, 7–13.

Cao, Y., Zhao, Y., Song, F., and Zhong, Q. (2014). Alkali metal cation doping of metal-organic framework for enhancing carbon dioxide adsorption capacity. *J. Energy Chem.* 23, 468–474. doi: 10.1016/S2095-4956(14)60173-X

Chang, P. H., Lee, T. J., Chang, Y. P., and Chen, S. Y. (2013). CO$_2$ Sorbents with Scaffold-like Ca-Al layered double hydroxides as precursors for CO$_2$ capture at high temperatures. *ChemSusChem* 6, 1076–1083. doi: 10.1002/cssc.201200910

Chen, C., Zhang, S., Row, K. H., and Ahn, W. S. (2017). Amine–silica composites for CO$_2$ capture: a short review. *J. Energy Chem.* 26, 868–880. doi: 10.1016/j.jechem.2017.07.001

Chen, H., Wang, W., Ding, J., Wei, X., and Lu, J. (2017). CO$_2$ adsorption capacity of FAU zeolites in presence of H$_2$O: a monte carlo simulation study. *Energy Proc.* 105, 4370–4376. doi: 10.1016/j.egypro.2017.03.929

Climent, M. J., Corma, A., Iborra, S., Epping, K., and Velty, A. (2004). Increasing the basicity and catalytic activity of hydrotalcites by different synthesis procedures. *J. Catal.* 225, 316–326. doi: 10.1016/j.jcat.2004.04.027

Flanigen, E. M., Lok, B. M., Patton, R. L., Wilson, S. T. (1986). *New Developments in Zeolite Science and Technology*. Tokyo: Co-Published by Kodansha LTD; Elsevier.

Hasegawa, K., and Matsumoto, A. (2017). Role of cation in target adsorption of carbon dioxide from CO$_2$-CH$_4$ mixture by low silica X zeolites. *AIP Conf. Proc.* 1865:020002. doi: 10.1063/1.4993321

Horbach, J., Chen, Q., Rennings, K., and Vögele, S. (2014). Environmental innovation and societal transitions do lead markets for clean coal technology follow market demand? A case study for China, Germany, Japan and the US. *Environ. Innov. Soc. Transit.* 10, 42–58. doi: 10.1016/j.eist.2013.08.002

Hutson, N. D., and Attwood, B. C. (2008). High temperature adsorption of CO$_2$ on various hydrotalcite-like compounds. *Adsorption* 14, 781–789. doi: 10.1007/s10450-007-9085-6

Li, R., Xue, T., Bingre, R., Gao, Y., Louis, B., and Wang, Q. (2018). Microporous Zeolite@vertically aligned Mg–Al layered double hydroxide Core@Shell structures with improved hydrophobicity and toluene adsorption capacity under wet conditions. *ACS Appl. Mater. Interfaces* 10, 34834–34839. doi: 10.1021/acsami.8b15118

Losch, P., Pinar, A. B., Willinger, M. G., Soukup, K., Chavan, S., Vincent, B., et al. (2017). H-ZSM-5 Zeolite model crystals : structure- diffusion-activity relationship in methanol- to-olefins catalysis. *J. Catal.* 345, 11–23. doi: 10.1016/j.jcat.2016.11.005

Lwin, Y., and Abdullah, F. (2009). High temperature adsorption of carbon dioxide on Cu-Al hydrotalcite-derived mixed oxides: kinetics and equilibria by thermogravimetry. *J. Therm. Anal. Calorim.* 97, 885–889. doi: 10.1007/s10973-009-0156-7

Mustapa, S. I., Leong Yow, P., and Hashim, A. H. (2010). "Issues and challenges of renewable energy development: a Malaysian experience," in *Proceedings of the International Conference on Energy and Sustainable Development: Issues and Strategies (ESD 2010)* (Chiang Mai: IEEE), 1–6. doi: 10.1109/ESD.2010.5598779

Ocampo, F., Cunha, J. A., Santos, M. R., de, L., Tessonnier, J. P., Pereira, M. M., and Louis, B. (2010). Synthesis of zeolite crystals with unusual morphology: application in acid catalysis. *Appl. Catal. A Gen.* 390, 102–109. doi: 10.1016/j.apcata.2010.09.037

Ocampo, F., Yun, H. S., Pereira, M. M., Tessonnier, J. P., and Louis, B. (2009). Design of MFI zeolite-based composites with hierarchical pore structure: a new generation of structured catalysts. *Cryst. Growth Des.* 9, 3721–3729. doi: 10.1021/cg900425r

Othman, M. R., Rasid, N. M., and Fernando, W. J. N. (2006). Mg-Al Hydrotalcite coating on zeolites for improved carbon dioxide adsorption. *Chem. Eng. Sci.* 61, 1555–1560. doi: 10.1016/j.ces.2005.09.011

Pham, T. D., Hudson, M. R., Brown, C. M., and Lobo, R. F. (2014). Molecular basis for the high CO_2 adsorption capacity of chabazite zeolites. *ChemSusChem* 7, 3031–3038. doi: 10.1002/cssc.201402555

Princiotta, F. (2011). *Global Climate Change - The Technology Challenge (Advances in Global Change Research 38)*. Springer.

Sharma, U., Tyagi, B., and Jasra, R. V. (2008). Synthesis and characterization of Mg–Al–CO_3 layered double hydroxide for CO_2 adsorption. *Ind. Eng. Chem. Res.* 47, 9588–9595. doi: 10.1021/ie800365t

Sircar, S., Golden, T. C., and Rao, M. B. (1996). Activated carbon for gas separation and storage. *Carbon N. Y.* 34, 1–12. doi: 10.1016/0008-6223(95)00128-X

Siriwardane, R. V., Shen, M. S., Fisher, E. P., and Losch, J. (2005). Adsorption of CO_2 on zeolites at moderate temperatures. *Energy Fuels* 19, 1153–1159. doi: 10.1021/ef040059h

Smil, V. (2017). *Energy Transitions: Global and National Perspectives, 2nd Edn.* Santa Bárbara, CA: Praeguer.

Stanley, M. (2003). *The Economics of Climate Change—A Primer*. The Congress of the United States. Avialable online at: https://www.cbo.gov

Veltman, K., Singh, B., and Hertwich, E. G. (2010). Human and environmental impact assessment of postcombustion CO_2 capture focusing on emissions from amine-based scrubbing solvents to air. *Environ. Sci. Technol.* 44, 1496–1502. doi: 10.1021/es902116r

Vericella, J. J., Baker, S. E., Stolaroff, J. K., Duoss, E. B., Hardin, J. O., Lewicki, J., et al. (2015). Encapsulated liquid sorbents for carbon dioxide capture. *Nat. Commun.* 6, 1–7. doi: 10.1038/ncomms7124

Wang, J., Mei, X., Huang, L., Zheng, Q., Qiao, Y., Zang, K., et al. (2015). Synthesis of layered double hydroxides/graphene oxide nanocomposite as a novel high-temperature CO_2 Adsorbent. *J. Energy Chem.* 24, 127–137. doi: 10.1016/S2095-4956(15)60293-5

Wang, Q., Tay, H. H., Zhong, Z., Luo, J., and Borgna, A. (2012). Synthesis of high-temperature CO_2 adsorbents from organo-layered double hydroxides with markedly improved CO_2 capture capacity. *Energy Environ. Sci.* 5, 7526–7530. doi: 10.1039/c2ee21409a

Xu, Y., Maddox, P. J., and Couves, J. W. (1990). The Synthesis of SAPO-34 and CoSAPO-34 from a Triethylamine–hydrofluoric acid–water system. *J. Chem. Soc. Faraday Trans.* 86, 425–429. doi: 10.1039/FT9908600425